Tomographic molecular imaging of x-ray-excitable nanoparticles

Guillem Pratx,[1] Colin M. Carpenter,[1] Conroy Sun,[1] Ravi P. Rao,[2] and Lei Xing[1,*]

[1]*Stanford University School of Medicine, Department of Radiation Oncology, 875 Blake Wilbur Drive, Stanford, California 94305-5847, USA*

[2]*SRI International, 333 Ravenswood Avenue, Menlo Park, California 94025, USA*

**Corresponding author: lei@stanford.edu*

Received May 19, 2010; revised August 9, 2010; accepted August 18, 2010; posted September 17, 2010 (Doc. ID 128623); published October 8, 2010

X-ray luminescence computed tomography (XLCT) is proposed as a new dual molecular/anatomical imaging modality. XLCT is based on the selective excitation and optical detection of x-ray-excitable nanoparticles. As a proof of concept, we built a prototype XLCT system and imaged near-IR-emitting Gd_2O_2S:Eu phosphors in various phantoms. Imaging in an optically diffusive medium shows that imaging performance is not affected by optical scatter; furthermore, the linear response of the reconstructed images suggests that XLCT is capable of quantitative imaging. © 2010 Optical Society of America

OCIS codes: 170.0110, 170.7440, 170.6960, 170.3880, 250.1500.

X-ray computed tomography (CT) is widely used for imaging the anatomy with high spatial resolution, but its use in molecular imaging remains limited. A few contrast agents, such as iodine or barium sulfate, can be imaged with CT, provided they are concentrated enough (>1 mg/ml) to produce a detectable signal [1]; however, more sensitive x-ray molecular agents are required for CT to become a useful tool in molecular imaging.

The development of phosphor nanoparticles (PNPs) [2–4] opens new possibilities for using x rays to image molecular tracers *in vivo*. When irradiated with x rays, some PNPs produce near-IR (NIR) light that can propagate through tissue and be measured by sensitive photodetectors [5]. X-ray luminescence (XL) is well characterized for bulk inorganic scintillators [6]. Briefly, by interacting with matter, an x ray produces a shower of energetic electrons that can activate luminescent centers in the phosphor and produce light. A single 100 keV x ray can produce on the order of 5000 photons, distributed around the primary ionization track, which can extend 100 μm. For dilute amounts of PNPs injected *in vivo*, light can be produced even if the x ray interacts in tissue, because energetic electrons can travel to nearby PNPs. Thus, the XL signal is proportional to the PNP concentration [5].

In principle, it is possible to apply bioluminescence tomography techniques to reconstruct the 3D distribution of the luminescent sources [7]. Yet, for a standard radiation dose, too few photons are produced for accurate reconstruction from such diffuse measurements. Instead, a selective excitation scheme is proposed for obtaining high-quality images from a limited number of photons. In this scheme, called x-ray luminescence computed tomography (XLCT), [8], the sample is irradiated by a sequence of narrow x-ray beams positioned at predefined locations, while photodetectors measure the XL signal (Fig. 1). Regardless of where photons are detected, it is known that those photons were created somewhere on the path of the x-ray beam. Hence, XLCT produces projective measurements similar to those recorded in conventional CT.

X-ray selective excitation was first introduced in x-ray fluorescence computed tomography (XFCT) [9]. In XFCT, the production of fluorescent x rays is stimulated by irradiating the sample with a narrow monochromatic beam. Recently, XFCT was used to image gold nanoparticles inside a water phantom [10]. However, the physical nature of the signals produced in XFCT and XLCT leads to different hardware designs and results in different imaging performance.

In this Letter, we report the first images obtained with XLCT. Two phantoms were fabricated by suspending various concentrations of a micrometer-sized Gd_2O_2S:Eu (GOSE) phosphor powder in a 1% agar gel solution. GOSE was used in this work as a proof of concept and is not proposed as an imaging tracer, due to its emission wavelength and toxicity. Recently, we have fabricated 10 nm $BaYF_5$:Eu PNPs, and observed strong XL at 700 nm [4].

The "turbid" phantom consisted of a 1 cm diameter, 2.5 cm high rod containing a 10 mg/ml concentration of phosphor embedded inside a 2.6 cm diameter, 4.5 cm high turbid cylinder. Titanium dioxide (2 g/l) and India ink (10 ml/l) were added to the gel to mimic the optical

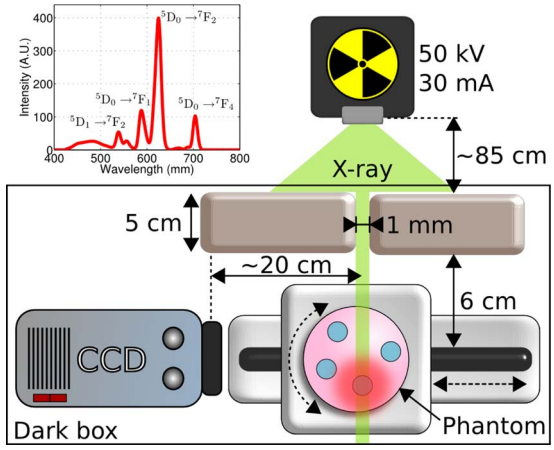

Fig. 1. (Color online) A phantom containing phosphor inclusions is moved on a rotation/translation stage while being irradiated by a narrow, stationary x-ray beam. At each position, the XL signal was measured with an EM-CCD camera. Inset, XL spectrum for GOSE.

properties of biological tissue [11]. Using optical tissue spectroscopy[12], we measured the optical attenuation and scatter coefficients of the turbid phantom over a wide range of wavelengths. For the strongest GOSE emission peak (627 nm), these coefficients were $\mu_a = 0.025\ \mathrm{cm}^{-1}$ and $\mu_s' = 7.8\ \mathrm{cm}^{-1}$, respectively. A "gradient" phantom was also fabricated by embedding eight 1 cm diameter rods containing various phosphor concentrations (0, 0.01, 0.05, 0.1, 0.5, 1, 5, and 10 mg/ml, respectively) inside a translucent 6.2 cm diameter, 4 cm high gel cylinder.

The XLCT acquisition was performed as follows. The x-ray source (Therapax SXT 150, Elimpex) voltage and current were set to 50 kV and 30 mA, respectively, and the beam was filtered with 0.4 mm Al (Fig. 1). The turbid phantom was translated 26 times in increments of 1 mm, and rotated 24 times to cover 360°. The larger gradient phantom was translated 55 times in increments of 1 mm, and rotated 30 times. For both acquisitions, the x-ray beam was collimated by two lead bricks separated by a 1 mm gap (Fig. 1). For each beam position, the unfiltered XL was measured with an electron-multiplying CCD (EM-CCD) camera (ImagEM C9100-13, Hamamatsu) using a $f/1.4$ lens, 512×512 pixels, an exposure time of 1 s, and an EM gain of 160 (Fig. 2). The image acquisition apparatus was enclosed in a light-tight box made of black hardboard, a material that does not substantially attenuate the x-ray beam. Although the CCD was shielded from direct x-ray interactions, secondary x rays produced hot spots in the images (Fig. 2). These hot spots were removed by a custom image processing method. In both experiments, a projection sinogram was formed by summing all the pixels together after correcting for dark noise. By running the CCD camera as a "single-pixel detector," we show that, in XLCT, image formation is based on a simple selective excitation scheme rather than complex optical measurements and reconstruction.

A rough correction was applied to the turbid phantom sinogram to compensate for the exponential attenuation of the XL signal with phantom position (Fig. 1). No such correction was applied to the translucent gradient phantom. Both sinograms were reconstructed with 100 iterations of the maximum-likelihood expectation maximization (ML-EM) algorithm, which models the physical response of the imaging system [13]. Computer simulations were also conducted using digital phantoms and an analytical beamlet model [8]. The simulations assumed monochromatic 627 nm light emission from GOSE and an ideal photodetector (no dark or read noise, 100% quantum efficiency).

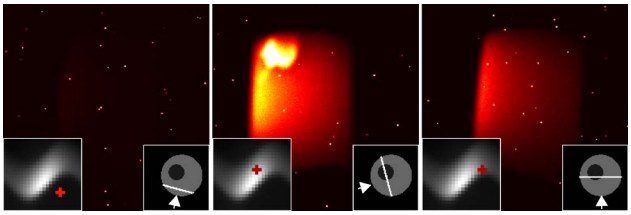

Fig. 2. (Color online) Sample images acquired with an EM-CCD camera (white arrow) of the turbid phantom under three different x-ray irradiations (bottom-right inset). Each image maps to a sinogram bin (red cross, bottom-left inset). The hot spot in the middle image was caused by a defect in the phantom.

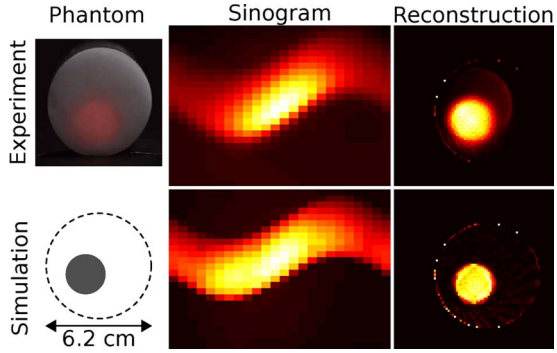

Fig. 3. (Color online) A turbid phantom (left), composed of phosphor suspended in an optically diffusive cylinder, was acquired using XLCT to produce a sinogram (middle), which was reconstructed with 100 iterations of ML-EM (right). The simulation (bottom row) modeled the light propagation in a diffuse medium.

In the turbid phantom, the XL signal undergoes strong optical scatter, yet the x-ray excitation encodes the position of the emitted photons with sufficient accuracy to reconstruct tomographic images with high fidelity (Fig. 3, top row). The shadow visible in the background of the reconstructed image is attributed to x-ray scatter. A simulation of the turbid phantom, which accounted for the propagation of 627 nm light in the diffusive medium, was also performed as a reference (Fig. 3, bottom row). Some of the differences between the simulation and the experiment are attributed to a defect in the turbid phantom, which was not simulated (Fig. 2, middle).

For the gradient phantom, the four most concentrated phosphor inclusions (0.5, 1, 5, and 10 mg/ml) were visualized in the XLCT images (Fig. 4). The weaker inclusions (0.01, 0.05, and 0.1 mg/ml) were not detected, likely because they were overshadowed by the brighter phosphor inclusions. Planar imaging of the gradient phantom in an IVIS 200 system (Caliper Life Sciences) using optical excitation showed that only the two most concentrated inclusions could be resolved (red overlay, Fig. 4, top left corner).

The XL signal was averaged within 1 cm diameter circular regions of interest drawn around each of the four visible inclusions. The reconstructed signal shows a linear response relative to the input GOSE concentration

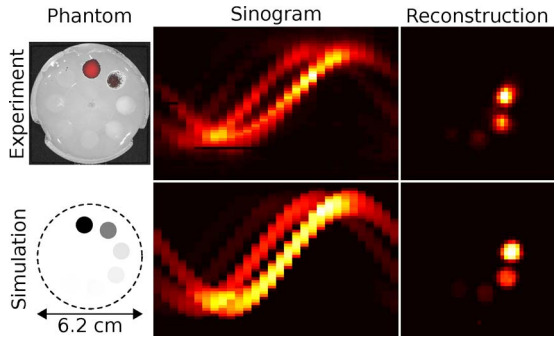

Fig. 4. (Color online) A gradient phantom (left), composed of various phosphor concentrations embedded in a gel, was acquired using XLCT to produce a sinogram (middle), which was reconstructed with 100 iterations of ML-EM (right).

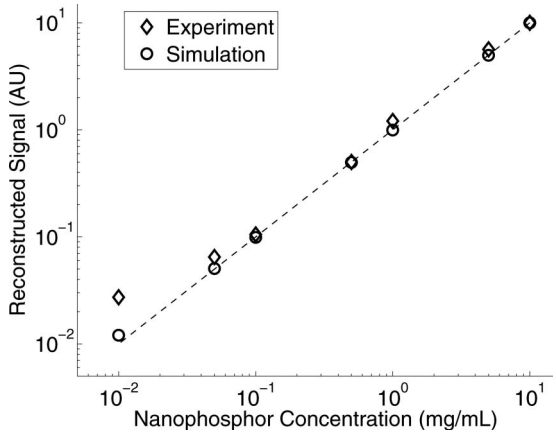

Fig. 5. Response linearity for all seven phosphor inclusions, shown for the experimental and simulated gradient phantom.

(Fig. 5), suggesting that XLCT is capable of quantitative imaging. Excluding the two weakest inclusions, the coefficients of determination were $R^2_{\mathrm{exp}} = 0.996$ and $R^2_{\mathrm{sim}} = 0.99999$, respectively.

Although spatially resolving optical detectors are not required for XLCT imaging, measuring the spatial distribution of the XL signal (Fig. 2) could provide additional information to improve image quality. For instance, hybrid reconstruction could combine models of tissue ionization by x-ray and light diffusion through tissue.

Compared to other molecular imaging modalities, XLCT possesses several advantages. First of all, it can produce anatomical and molecular images that are spatially and temporally registered. Furthermore, the spatial resolution of the images is mainly determined by the beam sampling and width and can be easily optimized. Similarly, the molecular sensitivity is proportional to the beam current and exposure time. However, a higher radiation dose is required for improving image quality, and there is a trade-off between sensitivity, spatial resolution, and radiation dose. In this study, for instance, the turbid and gradient phantoms received an average dose of 10 and 11 cGy, respectively.

The phosphor concentrations imaged in this study were also relatively high compared to typical nanoparticle uptake *in vivo*. For instance, biodistribution studies have shown uptake of quantum dots in various organs in the range of 5–50 μg/ml [14]. Although the range of concentrations in the gradient phantom was as low as 10 μg/ml, these were overshadowed by brighter inclusions. Based on Monte Carlo simulations, the XL signal produced by the 100 μg/ml inclusion is comparable to the level of background signal produced by x-ray scatter exciting the 10 mg/ml inclusion [8]. In addition, the maximum gain setting on the CCD camera was limited by the intensity of the brightest inclusion. Based on previous simulations, we expect phosphor concentrations as low as 1 μg/ml to be resolved with a radiation dose as low as 1 cGy [8].

Through experiments, we have shown for the first time (to our knowledge) that XLCT could image the cross-sectional distribution of x-ray-excitable PNP. These first XLCT images were produced with a rather simple experimental setup, and we expect image quality to improve with more precise experiments.

This work was supported by the National Science Foundation (NSF) (0854492), the National Cancer Institute In vivo Cellular and Molecular Imaging Centers (P50CA114747), and the Friends for an Earlier Breast Cancer Test Foundation.

References

1. U. Speck, in *Molecular Imaging I* (Springer, 2008), pp. 167–175.
2. M. Xing, W. Cao, T. Pang, X. Ling, and N. Chen, Chin. Sci. Bull. **54**, 2982 (2009).
3. Y. Tian, W.-H. Cao, X.-X. Luo, and Y. Fu, J. Alloys Compd. **433**, 313 (2007).
4. C. Sun, C. Carpenter, G. Pratx, and L. Xing, in *World Molecular Imaging Congress* (2010).
5. C. M. Carpenter, C. Sun, G. Pratx, R. Rao, and L. Xing, Med. Phys. **37**, 4011 (2010).
6. P. Lecoq, A. Annenkov, A. Gektin, M. Korzhik, and C. Pedrini, *Inorganic Scintillators for Detector Systems: Physical Principles and Crystal Engineering* (Springer, 2006).
7. W. Cong, G. Wang, D. Kumar, Y. Liu, M. Jiang, L. Wang, E. Hoffman, G. McLennan, P. McCray, J. Zabner, and A. Cong, Opt. Express **13**, 6756 (2005).
8. G. Pratx, C. Carpenter, C. Sun, and L. Xing, "X-ray luminescence computed tomography via selective excitation: a feasibility study," IEEE Trans. Med. Imag. (to be published).
9. R. Cesareo and S. Mascarenhas, Nucl. Instrum. Methods Phys. Res. Sect. A **277**, 669 (1989).
10. S.-K. Cheong, B. L. Jones, A. K. Siddiqi, F. Liu, N. Manohar, and S. H. Cho, Phys. Med. Biol. **55**, 647 (2010).
11. B. W. Pogue and M. S. Patterson, J. Biomed. Optics **11**, 041102 (2006).
12. T. H. Pham, O. Coquoz, J. B. Fishkin, E. Anderson, and B. J. Tromberg, Rev. Sci. Instrum. **71**, 2500 (2000).
13. L. A. Shepp and Y. Vardi, IEEE Trans. Med. Imag. **1**, 113 (1982).
14. N. Ma, A. F. Marshall, S. S. Gambhir, and J. Rao, Small **6**, 1520 (2010).